Original Article

UAV-mounted Ground Penetrating Radar: an example for the stability analysis of a mountain rock debris slope

Riccardo SALVINI¹* https://orcid.org/0000-0002-8506-4657; ✉ e-mail: riccardo.salvini@unisi.it

Luisa BELTRAMONE¹ https://orcid.org/0000-0003-0891-255X; e-mail: luisa.beltramone@unisi.it

Vivien DE LUCIA¹ https://orcid.org/0000-0001-6691-2991; e-mail: vivien.delucia2@unisi.it

Andrea ERMINI¹ https://orcid.org/0000-0002-6830-5586; e-mail: andrea.ermini@unisi.it

Claudio VANNESCHI² https://orcid.org/0000-0002-3285-6458; e-mail: claudio.vanneschi@regione.toscana.it

Caterina ZEI³ https://orcid.org/0000-0001-5838-9889; e-mail: zeicrn@unife.it

Daniele SILVESTRI¹ https://orcid.org/0009-0001-3596-3283; e-mail: daniele.silvestri@unisi.it

Andrea RINDINELLA¹ https://orcid.org/0000-0003-1627-9993; e-mail: rindinella@unisi.it

*Corresponding author

1 Department of Environment, Earth and Physical Sciences and Centre of Geotechnologies CGT, University of Siena, Via Vetri Vecchi 34, 52027, San Giovanni Valdarno (Arezzo), Italy

2 Direzione Urbanistica, Settore Sistema Informativo e Pianificazione del Territorio, Regione Toscana, Via di Novoli 26, 50127 Florence, Italy

3 Department of Physics and Earth Science, University of Ferrara, Via Giuseppe Saragat 1, 44122, Ferrara, Italy

Citation: Salvini R, Beltramone L, De Lucia V, et al. (2023) UAV-mounted Ground Penetrating Radar: an example for the stability analysis of a mountain rock debris slope. Journal of Mountain Science 20(10). https://doi.org/10.1007/s11629-023-8162-y

Abstract: This paper describes scientific research conducted to highlight the potential of an integrated GPR-UAV system in engineering-geological applications. The analysis focused on the stability of a natural scree slope in the Germanasca Valley, in the western Italian Alps. As a consequence of its steep shape and the related geological hazard, the study used different remote sensed methodologies such as UAV photogrammetry and geophysics survey by a GPR-drone integrated system. Furthermore, conventional in-situ surveys led to the collection of geological and geomorphological data. The use of the UAV-mounted GPR allowed us to investigate the bedrock depth under the detrital slope deposit, using a non-invasive technique able to conduct surveys on inaccessible areas prone to hazardous conditions for operators. The collected evidence and the results of the analysis highlighted the stability of the slope with Factors of Safety, verified in static conditions (i.e., natural static condition and static condition with snow cover), slightly above the stability limit value of 1. On the contrary, the dynamic loading conditions (i.e., seismic action applied) showed a Factor of Safety below the stability limit value. The UAV-mounted GPR represented an essential contribution to the surveys allowing the definition of the interface debris deposit-bedrock, which are useful to design the slope model and to evaluate the scree slope stability in different conditions.

1 Introduction

The development of remote sensing techniques has undergone a significant acceleration in the last decades with the advent of novel methodologies, the increase in their efficiency, and the high-performance hardware and software costs reduction. These advances allowed to improve the acquisition of a large amount of data without direct contact with the object of the analysis. In the experimental field, data may concern geometric characteristics of surfaces and objects which need to be investigated (e.g., 3D acquisitions either by aerial and ground-based laser scanning or photogrammetry).

The fields of application of these remote sensing techniques are various: from geology to engineering, from precision farming to environmental monitoring and archaeology. Indeed, geomatic techniques are becoming more transversal to various disciplines linked to georeferenced data that can be collected quickly and with high spatial resolution. Nevertheless, one of the main drawbacks of these techniques is the restricted exploration depth; so much so that most of them allow the investigation of the object' surface, without the possibility of exploring the underlying layers. This can be fundamental in certain contexts when it is necessary to either investigate the depth of soils and geological layers or to identify buried archaeological and engineering structures and/or artifacts.

Geophysical methods are usually used for this type of operations, such as seismic prospecting by refraction or reflection, geoelectric analysis, or interpretation of ground-based radar data. One of the main problems for these techniques lies in the need to operate in contact with the ground, which is not always possible for several reasons, including inaccessibility, safety (e.g., unstable landslide areas or forbidden areas), and land use (e.g., shrublands, stony and highly irregular soils or slopes). Therefore, integrated high-resolution remote sensing approaches with geophysical techniques, such as ground penetrating radar (GPR), have recently been developed. Typically, they involve the use of radar systems mounted or integrated into drones. This is possible thanks to the development of increasingly high-performance and relatively affordable unmanned aerial vehicles (UAV), capable of carrying payloads of a few kilograms while ensuring excellent flight time autonomy. Furthermore, technological development has made it possible to create small and light radar antennas capable of penetrating the surface even for a few tens of meters. The combination of UAV and GPR has been recently commercialized, and it is revolutionary in various application contexts allowing the acquisition of underground data remotely, safely, and quickly.

The GPR is an active sensor which allows to analyse the first layers of the subsoil by emitting electromagnetic waves at regular intervals of a certain frequency. When the centimetric electromagnetic waves meet a discontinuity in depth, they undergo partial reflection returning to the instrument and being recorded by a receiving antenna which analyses their characteristics. A discontinuity implies a dielectric change due to the variation in the object's properties or in the crossed layers (Jol 2009). By the use of specific algorithms based on wave phase and amplitude, travel time, and hypotheses on the dielectric coefficient of the crossed medium, it is possible to calculate the depth where this reflection occurs. In this context, the higher the frequency of the emitted wave, the greater the spatial resolution, or the detail obtainable, with the possibility of identifying even small objects or thin layers. The drawback of a greater spatial resolution is a reduced ability to penetrate in depth (from a few decimetres to a few metres). On the contrary, low-frequency antennas can investigate the ground at great depths (even over a few tens of meters) at the expense of the obtainable detail (Jol 2009).

Since the GPR needs direct contact with the surface to be investigated, its traditional applications are mainly focused on archaeological surveys (Qin et al. 2018; Novo et al. 2021; Hall et al. 2022; Abudeif et al. 2022; Al-Ruzouq et al. 2022), snow and ice thickness analysis in mountains or extreme environments (Feiger et al. 2018; Liu et al. 2020; Guo et al. 2022), definition of bedrock depth and underground reconstruction (Shukla et al. 2013; Azahar et al. 2018; Nath et al. 2018; Diallo et al. 2019; Tomecka-Suchoń et al. 2019; Onyebueke et al. 2022), fractures identification (Elkarmoty et al. 2018; Grandjean and Gourry 1996; Kulich and Bleibinhaus

2020; Zanzi et al. 2019), definition of ground and underground water contamination (Wang and Tan 2018; Guireli Netto et al. 2020; Maryadi et al. 2020; Fuente et al. 2021; Sonkamble and Chandra 2021; Yun et al. 2021; Gomes et al. 2022), and ground water protection (Peterson and Doliber 2019; Zajc and Urbanc 2019; Essam et al. 2020; Hussain et al. 2020).

In the last decade, particularly from 2016 (Miccinesi et al. 2022), there was a growing commercialization of drones that led to an increasing number of studies related to their scientific applications, including GPR and synthetic aperture radar (SAR). Parallelly, the technological progress has led the development of GPR systems that can be used remotely with an extremely high signal-to-noise ratio. Some examples of this upgraded configuration are mainly related to landmine detection (Garcia-Fernandez et al. 2018a; Garcia-Fernandez et al. 2019a, 2019b; Garcia-Fernandez et al. 2022; Šipoš and Gleich 2020), snowpack and glaciology research (McCallum and Fairweather 2013; Tan et al. 2017; Briggs et al. 2018; Eckerstorfer et al. 2018; Jenssen et al. 2020; Prager et al. 2022; Vergnano et al. 2022; Emilsson et al. 2022), agricultural research (Wu et al. 2019; Hou et al. 2021), archaeological survey (Yarleque et al. 2017; Colica et al. 2022), soil characteristics under railways mapping (Bayisa et al. 2015), investigation of water and sediment depths of lakes and rivers (Bandini et al. 2022), and buried objects detection (Ludeno et al. 2017).

Additional studies about the presence of rock discontinuities were carried out by Zhao et al. (2022) and Saponaro et al. (2021) following the survey approach adopted in the present research and coupling digital photogrammetry and GPR through an integrated drone system.

These examples of utilizing GPR mounted on drones illustrate how this configuration can serve not only as a non-destructive survey tool for significant sites but also as an asset in hazardous situations or locations, safeguarding both specialized personnel and civilians. Moreover, the utilization of this configuration offers enhanced efficiency in terms of both safety and time, particularly in hazardous and challenging terrains where the conventional trolley-mounted GPR survey is unfeasible.

The current case study, focused on the utilization of a drone-based GPR, aimed experimentally to explore the integration of this technique for slope stability assessment. Such a combination of methodologies is up to today seldomly encountered due to several constraints including instrumentation costs, morphological conditions and the presence of obstacles. The main reason behind the necessity to couple the GPR with the drone is related to the survey conditions of the presented case study: the area is characterised by mountain landscape with vertical rocky slopes overhanging steep talus versants made up of blocks with various dimensions and volumes, fine materials, and scattered vegetation (i.e., grass, bushes, and trees). In addition, the precipitous steepness and the lack of footpaths along the slopes make the area hardly accessible by foot and dangerous for operators. For these reasons, the GPR-UAV configuration was the best fit to survey efficiently the area and find the interface debris deposit-bedrock, avoiding any potential danger to operators.

2 Geological Framework

The slope under study is located in the Western Piedmont Region (Province of Turin, Italy), in the Dora-Maira Massif (Cottian Alps – Fig. 1).

The Germanasca Valley has a doubled morphological trend: a first part SSW–NNE trending and a second one E–W trending. The valley, in the proximity of the study area, has a minimum altitude of about 1,000 m and a maximum of 1,550 m a.s.l.

From a geological perspective, the area is located in the Dora-Maira Unit which belongs to the subdomain of the Internal Crystalline Massifs of the Pennidic Domain, the axial part of the Western Italian Alpine chain. The Pennidic Domain (Fig. 1) is characterized by the highest metamorphism and the most intense and complex deformations, and it is divided into various subdomains including the Internal Crystalline Massifs (i.e., Dora-Maira, Gran Paradiso and Monte Rosa), the Piedmontese, Briançonnais, and Sub-Briançonnais zones.

In particular, the rocks present in the study area belong to the Dora-Maira Massif (DM2 in Fig. 1) which is characterised by lithologies of the Polymetamorphic Complex. The latter is made up of micaschists, with variable petrographic compositions, and the presence of impure marble and orthogneiss. The Quaternary deposits are represented by eluvial–colluvial deposits, screes, and large blocks (Fig. 2).

Most of the slopes are characterized by the
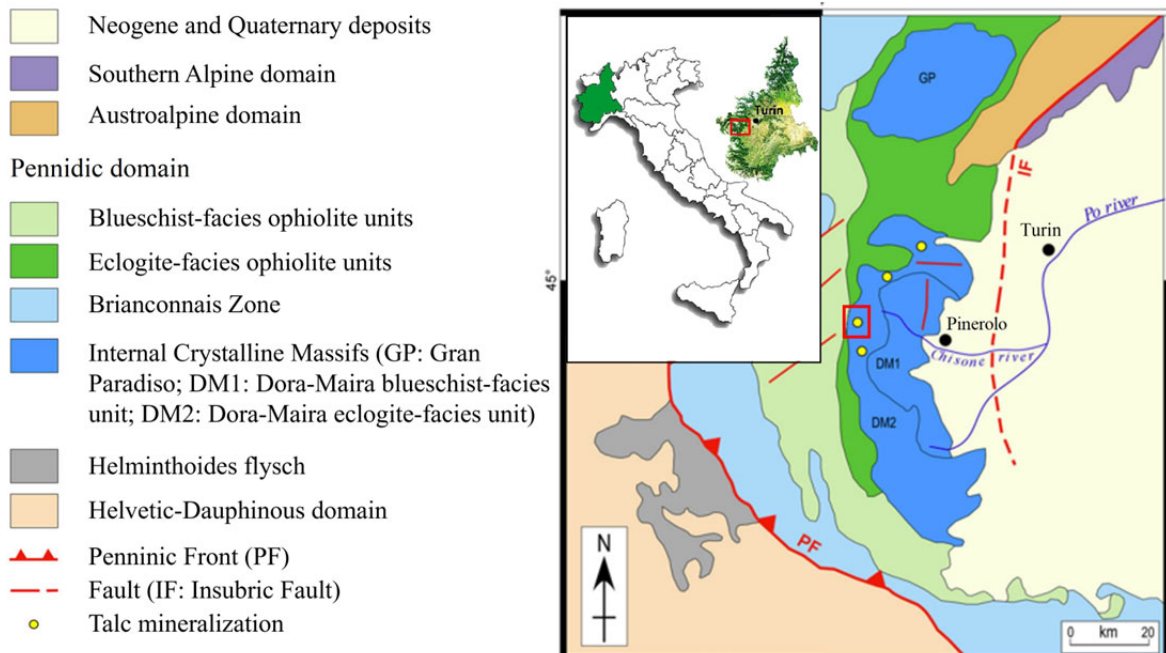
Fig. 1 Tectonic map of the Western Alps (modified from Cadoppi et al 2016). The inset map describes the localization of the study area in the Piedmont Region, Italy. The study area is indicated by the red rectangle.
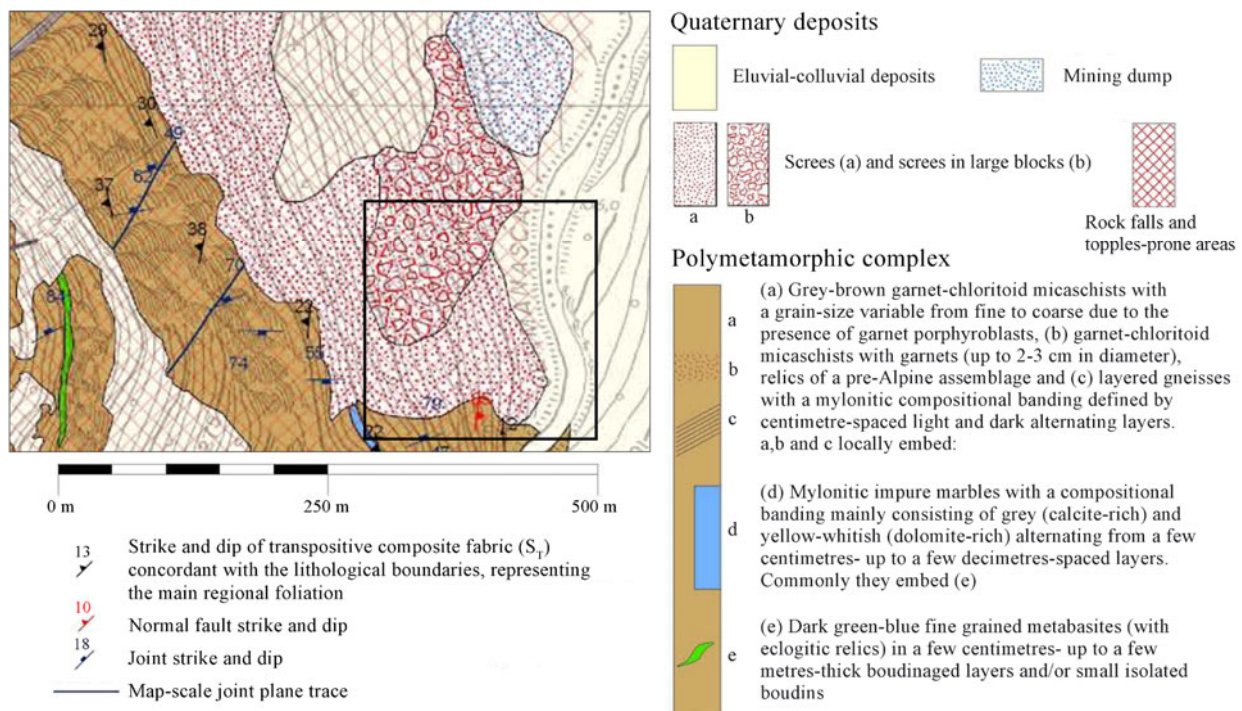
Fig. 2 Geological map of the study area (modified from Camanni 2010). The study area is indicated by the black rectangle.

presence of eluvial-colluvial deposits that often overlay directly the micaschists of the bedrock. The thickness of the deposits is difficult to assess but it certainly varies a lot, from a few tens of centimeters in moderate-slope areas at high altitudes – where soil develops directly on the rocky substrate – up to a few meters at the base of the escarpments. They consist of detrital material of various grain sizes with an almost absent fine matrix. The colluvial detrital deposit can be both non-vegetated or partially covered by shrubs

and sparse woodland. The deposit consists of angular blocks with a volume generally lower than a cubic meter, made up of micaschists of the Polymetamorphic Complex. The spread of debris is also conditioned by the presence of the overlying rock mass and its state of fracturing (Vanneschi et al. 2022). In fact, along the slopes there is also a lot of detritus in large blocks with chaotic accumulations due to mass gravitational processes due to collapse. Given the size of the elements and the position of some accumulations with respect to the feed areas, the influence of seismic events in determining the detachment of the blocks from the walls cannot be excluded (Bertea 1989). Alluvial deposits – consisting of heterometric gravels and rounded blocks – are also mapped along the valley of the Germanasca stream. Large block deposits have been identified within the riverbed, probably the result of the combined action of rock fall and of its transport along the watercourse during heavy flooding.

The stability of the scree slope under study was studied in static and dynamic conditions (i.e., seismic event). The simulation included the seismic hazard analysis which was based on Regional Legislation (D.G.R. n. 6-887 UPCM 3519/2006 of December 30th, 2019). The study area belongs to the municipality of Prali (red rectangle in Fig. 3) and presents a seismic hazard of class "3s" indicating a low seismic hazard. Nevertheless, the area may be exposed to modest shaking, having a maximum horizontal acceleration value (ag) varying between $0.125g$ and $0.150g$ with a probability of exceeding about 10% in 50 years (D.G.R. n. 6-887 UPCM 3519/2006 of December 30th, 2019).

3   Materials and Methods

3.1 In-situ surveys

3.1.1   Topographic and photogrammetric surveys

In the present case study, due to the area extension (about 4 ha), slope acclivity, and the general dangerous conditions for accessibility (steep slope made of blocks, with varied sizes and volumes, diversified vegetation, and the lack of footpaths) the surveys were conducted coupling drone flights and geological field checks.

The topographic survey, aimed to scale and to georeference the photogrammetric data, was conducted using two global navigation satellite system (GNSS) receivers (model Leica© GS15) and one Leica© Nova MS50 total station (TS).

The photogrammetric survey was carried out using a DJI© Mavic 2 Pro drone equipped with a Hasselblad© L1D-20C RGB camera characterised by a 10.26 mm lens and a 1" sensor offering a resolution of 20-megapixel. The flight aimed at obtaining the 3D digital dense point cloud, the digital dense elevation

National criteria	
Zone	PGA 475 (ag)
1	$0.25g < ag \leq 0.35g$
2	$0.15g < ag \leq 0.25g$
3	$0.05g < ag \leq 0.15g$
4	$\leq 0.05g$

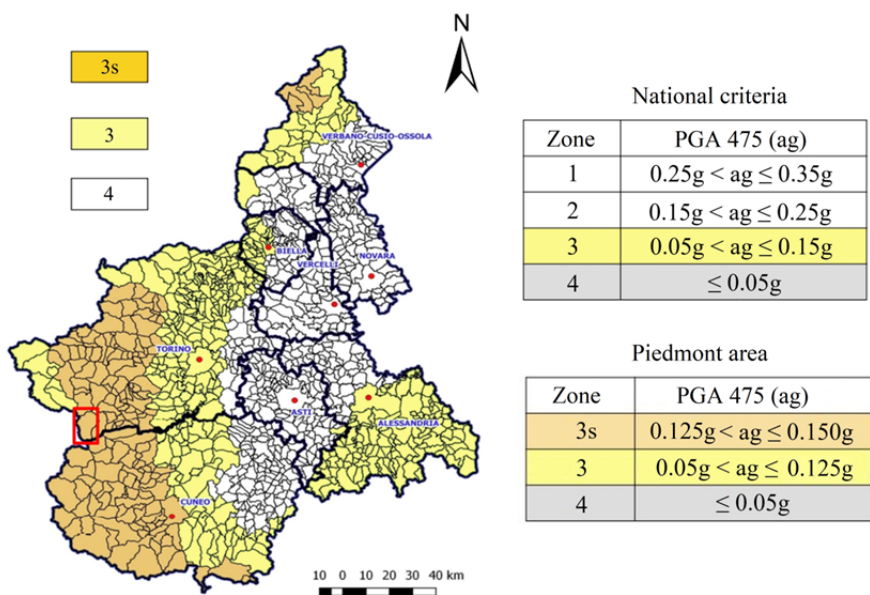| Piedmont area	
Zone	PGA 475 (ag)
3s	$0.125g < ag \leq 0.150g$
3	$0.05g < ag \leq 0.125g$
4	$\leq 0.05g$

10 0 10 20 30 40 km

Fig. 3 Seismic zoning map of Piedmont Region (modified from D.G.R. n. 6-887 UPCM 3519/2006 of December 30th, 2019). Acronyms PGA and ag indicate "peak ground acceleration" and "maximum horizontal acceleration value", respectively. The red rectangle indicates the municipality of Prali (Province of Turin).

model (DDEM), the digital dense terrain model (DDTM) and the orthophotomosaic of the slopes, both looking from frontal and nadiral directions.

The detailed description of topographic and photogrammetric surveys and their obtained results have been already published by Vanneschi et al. (2022). The area considered in the present study (Fig. 2) is a subset of that presented in Vanneschi et al. (2022).

3.1.2 Geophysical survey by the GPR-drone integrated system

In this work, a Cobra Plug-In GPR model, with a SubEcho 150 antenna characterized by a bandwidth (BW) of 260 MHz and a central frequency (CF) of 124 MHz, was used. The GPR antenna transmits electromagnetic waves to the ground and records reflections obtained when the signal encounters discontinuity surfaces, which may be present up to some meters deep. The antenna records these reflections and transmits data to the Prism2© software set in acquisition mode. Nowadays, the device can also be connected to a differential GNSS receiver, which allows to record the flight path and the antenna points of acquisition. In this work, a UAV-GPR configuration was used for detecting the interface depth between the debris covering the slope and the underlying bedrock. The radargram obtained was subsequently analysed and interpreted to identify the surface separating the geological layers. The survey was conducted by means of the GPR, equipped with a monostatic antenna and mounted on a DJI© Matrice 600 Pro drone (Fig. 4).

The SE–150 GPR was set up with a relative dielectric permittivity (RPD – i.e., the ability to store energy from an electromagnetic field and its transmission) equal to $\xi_r = 9$ MHz. Considering a ratio between the bandwidth range and the central frequency (BW/CF) equal to 210%, in light of the selected RPD, the vertical resolution resulted in 21 cm, whilst the horizontal one resulted in 59 cm.

The data acquisition system was composed by the COBRA Plug-in GPR-system and a wireless unit for real time sampling in 32 bits. A data logger was mounted on the drone granting GPR data recording and instrument control from the ground station. The drone was equipped with an automatic terrain following option using a laser/radar altimeter for altitude detection with high precision. During the GPR acquisition survey, the flight height was kept constant at a low altitude by the drone operator through manual altitude control (with an average height of 0.5 m from the ground surface) to guarantee a sufficient signal-to-noise ratio in view of the fact that air has zero mS/m conductivity.

The Cobra DAQ© software was used for GPR data acquisition by setting the Bluetooth technology for signal ringing reduction. In this study, the UAV-GPR survey was conducted along a 110 m path at the base of a debris slope as shown in Fig. 5A, Fig. 5C and Fig. 5D.

Fig. 4 COBRA Plug-in GPR Model SE–150 and DJI© Matrice 600Pro drone.

Additional UAV-GPR surveys were conducted in proximal areas at different heights along the slope, but they cannot be shown publicly due to a non-disclosure agreement with a neighbouring private company. Moreover, GPR path did not follow the slope profile for the stability analysis, due to the presence of vegetation and rock blocks and boulders that would have made the UAV survey problematic and dangerous if the suggested fly height of about 0.5 m was respected.

Data acquisition was conducted in continuous mode, with a constant offset between transmitted and received signals, and with a sampling interval between traces of 10 cm on the ground. The latter was automatically computed by the software using the integrated GNSS positioning working in differential modality thanks to a reference base properly set up on the ground. The GPR antenna was set up with an
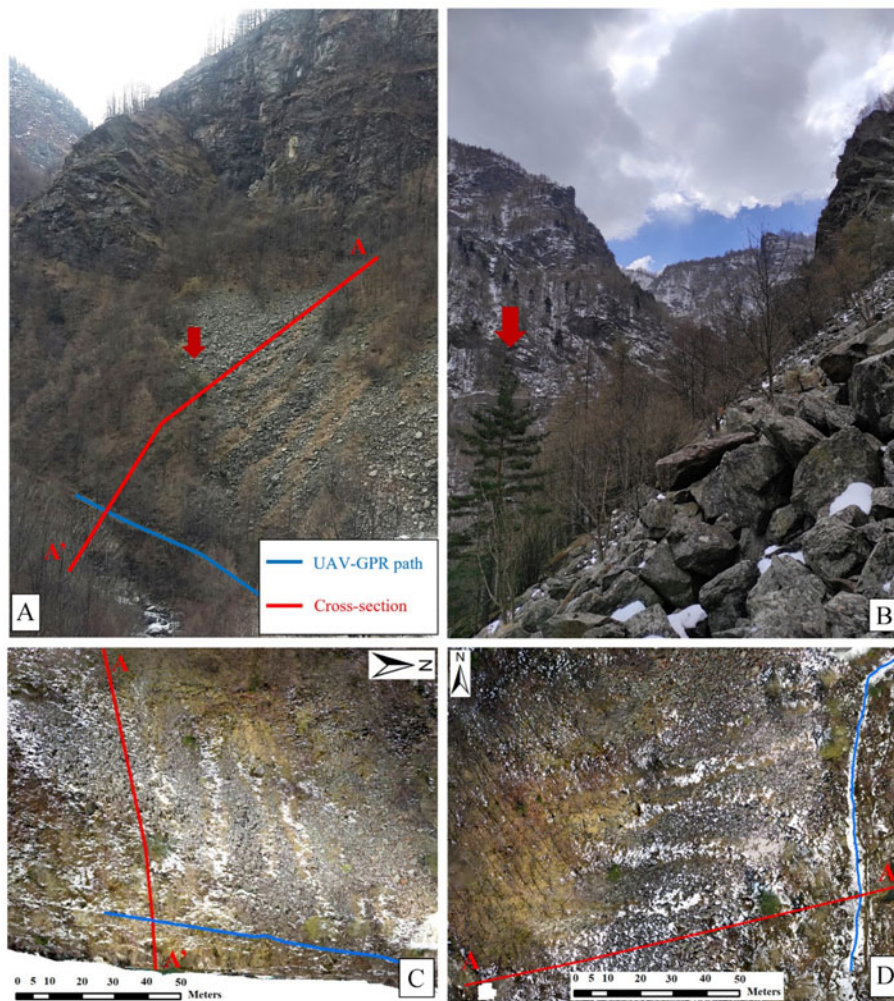
Fig. 5 Perspective view of the whole slope under study (A): the red arrow is meant to be a reference element (i.e., tree) for pictures A and B. Image B shows a detail of the debris deposit covering the slope, with blocks and boulders of different dimensions, and vegetated areas (i.e., grass, bushes and trees). Frontal orthophoto (C) and the nadiral orthophoto (D) of the studied area. The blue lines indicate the UAV-GPR path, while the red ones indicate the cross-section used for the slope stability analysis (A-A').

acquisition time of 470 ns after considering the characteristics of the study area.

The resulting raw radargram was subsequently processed using Prism2 software (version 2.70 - Radar Systems Inc. 2021). The main phases of the raw data processing were the "background removal" and the "Ormsby bandpass filter", needed to respectively reduce the background and the low-frequency noise. The automatic gain was adjusted in order to equalize the amplitude of the signal due to the attenuation that it undergoes with depth. The radargram processed so far is represented by a continuous flat cross-section which does not indicate the real correct depth and position of interfaces between the detrital deposit and the bedrock (Zhang et al. 2014); forasmuch, a topographic correction was applied using the

altimetric data stored by the GPR-GNSS integrated system.

3.2 Materials characterization and methods for slope stability analysis

The slope under study, due to the presence of different lithologies and particle sizes, – as shown in the geological-structural map of Fig. 2 – can be considered as a system characterised by a notable geotechnical complexity. Since in similar conditions a constitutive law valid in absolute terms is difficult to be addressed, simplified hypotheses are generally adopted in order to describe the materials behaviour and how it influences the stability of a given slope. For this reason, constitutive laws are generally used, such

as the Mohr-Coulomb failure criterion (Coulomb 1973), where the shear strength (τ_f) of a given material at failure is expressed by the parameters of cohesion (*c*) and friction angle (φ). These are considered constant for a given material in a specific condition and descriptive of an elastic-perfectly plastic model according to the following Eq. (1):

$$\tau_f = c + \sigma_n \tan (\varphi) \qquad (1)$$

where σ_n represents normal stress.

This failure criterion is simple and largely used and, even if not very suitable when describing the non-linear behaviour of intact rock, it well approximates the behavior of soils and, with a greater approximation, that of fractured rock. In the present case study this failure criterion was adopted for the bedrock and detrital deposit which constitutes the slope cover, since it has a behaviour comparable to that of a granular soil.

The slope stability analysis was undertaken according to the Limit Equilibrium method, which consists of studying the equilibrium of a rigid body sliding on a surface of any shape. The ratio between the available shear strength (τ_f), as computed according to Eq. (1), and the total shear stresses (τ) acting on a given slope, gives a preliminary assessment of stability through the factor of safety (FoS) according to the following Eq. (2):

$$\text{FoS} = \tau_f / \tau \qquad (2)$$

Consequently, a FoS > 1 implies a condition of stability, while a FoS < 1 is theoretically impossible and represents instability.

Moreover, in order to consider the presence of trees and low undergrowth in the slope under study (Fig. 5A and Fig. 5B) and their influence on the slope stability, the role of roots in influencing the cohesion was included in the computation. Many researchers have estimated the value of "root cohesion" for different vegetation species growing in different environments and their effect on slope stability (Chok et al. 2015; Sarkar et al. 2016). In particular, authors claim that the increase in soil shear strength due to root reinforcement is considered as an increase in apparent soil cohesion, called root cohesion, c_r. Therefore, it can be added directly to the terrain cohesion for versants which are interested by the presence of plant roots. The vegetation and its root system can provide additional apparent cohesion (Coppin and Richards 2007) due to their properties and characteristics being high tensile strength, adhesion properties and closely spaced root matrix

system (Chok et al. 2015). Differently, the root effect on friction angle can be considered negligible (Gray and Leiser 1982).

For this case study, the detrital deposit covered by grass, a cohesion value of 2.1 kPa was assigned. On the other hand, non-vegetated areas, a 0 kPa cohesion value, typical of granular non-coherent material was assigned. Furthermore, zones covered by trees, which majorly contribute to the increase of cohesion for the presence of a more robust roots system, a value of 3 kPa was assigned. The selected value of 2.1 kPa takes reference from root cohesion in slopes covered by grasses, sedges, and shrubs, while the value of 3 kPa to those covered by red alder, hemlock, Douglas fir, cedar as described in Buchanan and Savigny (1990).

Grass and tree roots can grow from a few inches to some meters from the surface, even though some tree roots can reach even further depth. Hence, root cohesion, in vegetated zones of the slope under study, was added approximately to the first two meters of depth where the radical apparatus can have an influence on material strength.

According to Chok et al. (2015) the Mohr-Coulomb equation can be modified to consider the root effect contribution in increasing the terrain shear strength as shown in Eq. (3):

$$\tau_f = c + c_r + \sigma_n \tan (\varphi) \qquad (3)$$

To assign the physical-mechanical properties to the involved materials, the geotechnical parameters as reported in the Inter-municipal Master Plan of the "Comunità Montana del Pinerolese" (2015) were considered as reference. The data reported in the Master Plan include the materials average geotechnical characteristics (as shown in Table 1) and a lithotechnical and hydrogeological map at a scale of 1:10,000.

Table 1 Geotechnical parameters of materials (detrital slope deposit and bedrock) involved in the study. The value of the cohesion for the detrital slope deposit is referred to as the total cohesion $c_t = c + c_r$.

Materials	γ (kN/m³)	Φ (°)	c_t (kPa)
Eluvial-colluvial deposits	16	35	5.0
Eluvial-colluvial deposits covered with trees	16	35	8.0
Scree with large blocks	17	42	0.0
Scree	17	40	0.0
Scree covered by grasses	17	40	2.1
Scree with trees	17	40	3.0
Scree with large blocks and trees	17	42	3.0
Micaschists	25	30	300.0

Note: γ, Unit weight; φ, Friction angle; c_t, Total cohesion.

The scree slope stability analysis was performed using RocScience© Slide2 software (RocScience Inc. 2022). The adopted calculation approach, available within the software environment, is the Simplified Bishop method (Bishop 1955).

Considering the size of the debris deposit and its high permeability, the analysis was conducted taking into account the fact that rainwater tends to permeate through the debris made up of large and irregular blocks, reaching the surface of the underlying bedrock.

As far as stability assessment is concerned it was decided to include dynamic forces, such as those due to seismic action. This should be evaluated, as indicated by the Italian Technical Standards for Construction ("Norme Tecniche per le Costruzioni NTC2018", NTC 2018), by using the "pseudo-static approach". This approach, among the other rules, states that the earthquake must be represented as an equivalent static action, constant in space and time, and proportional to the weight of a potentially unstable rock block.

Seismic parameters to be used in modelling were obtained from Geostru© PS 2018, a free online application (GeoStru 2022) able to provide the seismic hazard and the relative parameters for any given area within the Italian territory. The selected parameters are shown in Table 2, and they were chosen with reference to the following conditions: i) state life safety limit (stato limite di salvaguardia della vita - SLV) for a class of use type II and a reference period of 50 years, ii) topographic category T4, and iii) subsoil category B (NTC 2018; GeoStru 2022).

Table 2 Seismic parameters selected for the dynamic slope stability analysis according to the "pseudo-static approach"

Parameters	Value
Amax (Maximum acceleration) – m/s²	2.212
Kh (Horizontal seismic coefficient) (−)	0.054
Kv (Vertical seismic coefficient) (−)	0.027

Moreover, given the alpine location of the area, the possible additional load given by the snow on the ground was decided to be taken into consideration for a more realistic modelling of the conditions over several months of the year. In order to define the snow load to be applied on the slope surface, the Italian Technical Standards for Construction (NTC 2018) provide the following Eq. (4):

$$q_s = q_{sk} \cdot \mu_i \cdot C_E \cdot C_t \qquad (4)$$

where q_s is the snow load on the surface, q_{sk} is the value of the snow load at the ground (kN/m²) related to 50 years return period, μ_i is the surface shape coefficient, C_E is the exposure coefficient, and C_t is the thermal coefficient.

Since the last three parameters must be considered for the snow load calculation on building covers, they were omitted from the computation that was conducted only contemplating the snow load at the ground (q_{sk}). Due to the fact that the altitude of the study area is about 1,000 m a.s.l., according to NTC (2018), it must be classified as Zone 1 "Alpine"; in this case, Eq. (5) must be adopted for the q_{sk} calculation:

$$q_{sk} = 1.39 \cdot [1 + (a_s / 728)^2] \qquad (5)$$

where a_s is the site elevation (a.s.l.). The snow load acting on the slope resulted equal to 4.01 kN/m² and it was applied as constant along the slope, as a precaution, despite the modest variations in slope along the versant and the presence of sporadic trees leafless in the studied period.

Once the parameters for the seismic action and the snow load on the ground had been defined, the dynamic analyses on the debris slope stability were conducted thanks to the Slide2© software along the morphological profile created as described in the following paragraph.

3.3 Slope model creation

The 3D point cloud obtained from the UAV photogrammetric survey allowed to create the DDTM and to rebuild the natural slope morphology.

The elaboration was conducted using the open-source software for three-dimensional data processing CloudCompare (version 2.9.1 - GPL Software 2022). In this paper, as a demonstrative case of the UAV-GPR integrated system potentialities, a representative profile of the scree slope under study was chosen. Then, the 3D point cloud was utilized to extract a cross section in *.dxf format. The point cloud density led to a highly detailed morphological reconstruction of the entire slope. Despite this apparent advantage, provided by high-spatial-resolution modelling, when executing stability analysis, the latter can be excessive and problematic for the reliability of results. Usually, whether the case study is approached with Limit Equilibrium methods or more advanced numerical modelling, the stability analysis should be conducted on a simplified but representative significant

geometry. Fig. 6A shows the simplified version of the profile whose trace is represented by the red line in the orthophoto (Fig. 6B). The length of the created polyline determined the slope morphological profile and the vertical sides of the model. The bottom boundary of the cross section was interpreted taking into account the presence and the depth of the debris deposit and bedrock. Three principal areas, with different average dips of the scree deposit, were identified along the simplified slope model (Fig. 6).

The slope profile was imported into Slide2© and it allowed to create a model which includes the geological layers and their characteristics (Fig. 7). The

model was designed considering:

- the interpretation of the geological-structural maps: Camanni (2010), at a scale of 1:5,000, and "Comunità Montana del Pinerolese" (2015), with relative lithotechnical information, at a scale of 1:10,000;

- the field survey and the orthophoto interpretation for the localization of vegetated areas, in order to assign adequate total cohesion values;

- the results obtained by the GPR survey for the definition of the interface depth between debris deposit and micaschists bedrock;

- the water surface recognisable in the Germanasca stream and interpreted below the debris
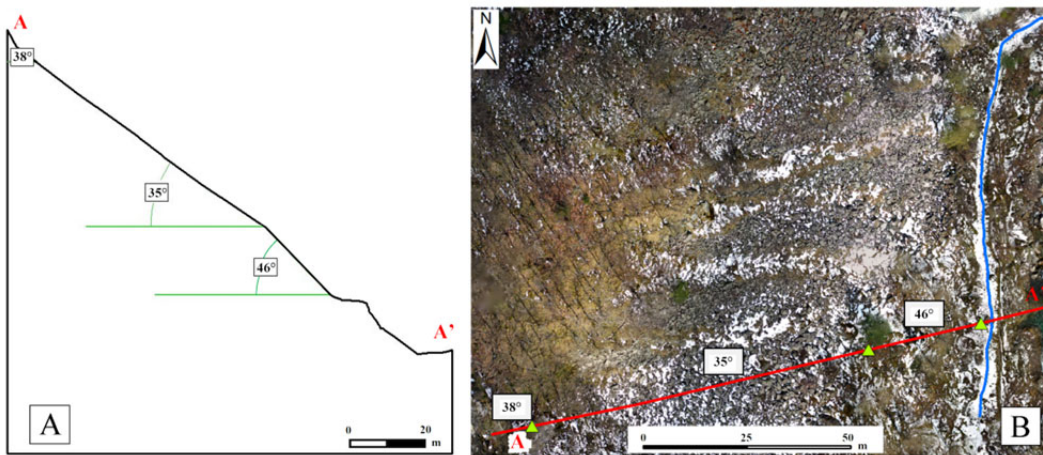

Fig. 6 (A) Slope profile as derived from the simplification of the 3D point cloud used for the stability analysis within Slide2©. (B) Trace of the slope profile A–A' (red line) with the nadiral orthophoto in background. The green triangles separate three main trends of dip value, respectively 38°, 35°, and 46° from the top to the bottom of the slope.
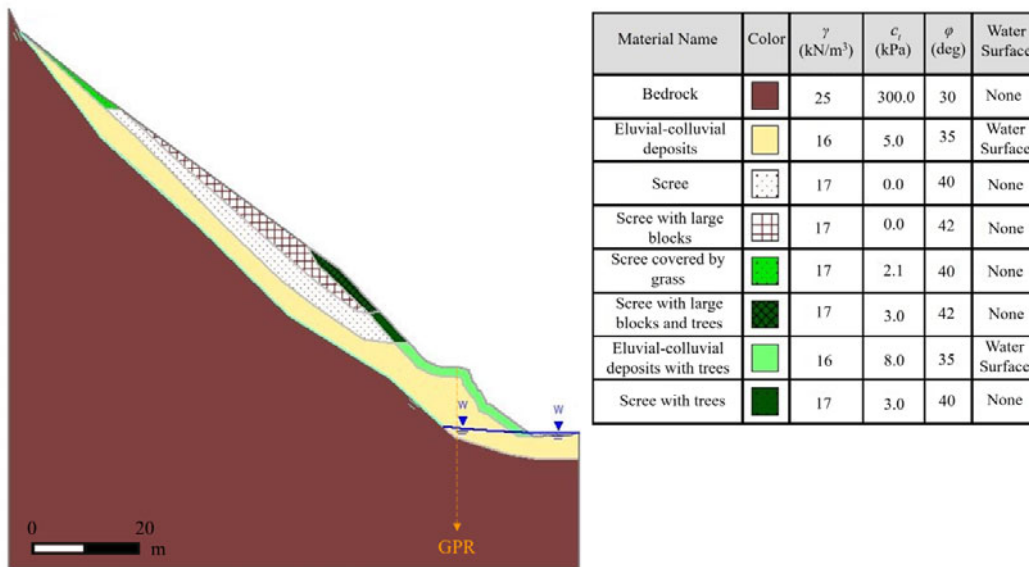

Material Name	Color	γ (kN/m³)	c_t (kPa)	φ (deg)	Water Surface
Bedrock		25	300.0	30	None
Eluvial-colluvial deposits		16	5.0	35	Water Surface
Scree		17	0.0	40	None
Scree with large blocks		17	0.0	42	None
Scree covered by grass		17	2.1	40	None
Scree with large blocks and trees		17	3.0	42	None
Eluvial-colluvial deposits with trees		16	8.0	35	Water Surface
Scree with trees		17	3.0	40	None

Fig. 7 Slope model designed in Slide2© and geological-lithotechnical properties assigned to the materials. The orange dashed line indicates the radargram trace, the blue line indicates the water surface, while the cyan line indicates the rainwater that permeates through the debris.

deposit due to the lack of hydrogeological data (blue line in Fig. 7);

- the rainwater that permeates through the debris, characterised by high permeability, and reaches the bedrock (cyan line in Fig. 7).

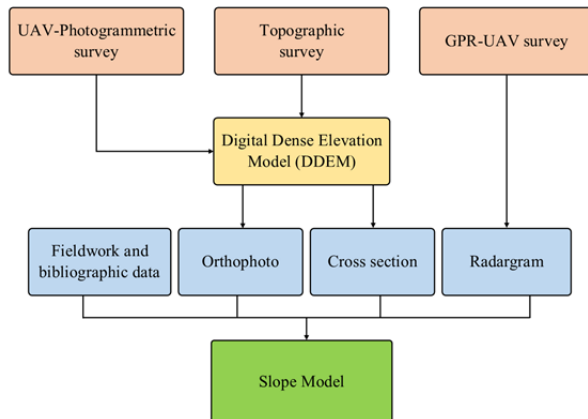In Fig. 8, the flowchart that summarizes the entire work process is shown.

Fig. 8 Flowchart of the proposed rock debris slope stability analysis.

4 Results

4.1 Topographic and photogrammetric survey

Even though the topographic and photogrammetric surveys were widely described and discussed in previous research by the same Authors (Vanneschi et al. 2022), for the sake of completeness it was considered necessary to sum up the obtained results to clarify the spatial accuracy of the data used in this research. The results can be summed up in two points:

1. The topographic survey aimed at georeferencing the data in the ETRF2000/UTM32N reference system through the measurement of artificial and natural targets. Natural targets, measured on the slope by the TS, showed a spatial accuracy of 3.8 cm, while artificial targets, measured by a GNSS-RTK survey (real time kinematic), showed spatial accuracies of 1 cm (horizontal accuracy) and 1.2 cm (vertical accuracy).

2. The processing of photogrammetric RGB data from UAV flights resulted in a final root mean square error (RMSE) of about 15 cm. Given the complexity and the extent of the area, the RMSE, even if not very low, was considered adequate for the rest of the analysis. From the images exterior orientation,

a 3D point cloud of the slope was created with a density of about 300 points/m². The latter permitted to interpolate a DDTM with a spatial resolution of 10 cm/pixel. Finally, the photographic images were orthorectified, and the orthophotomosaics, both in frontal and nadiral look direction, were created with a ground sampling distance (GSD) of 4 cm/pixel.

4.2 UAV-GPR survey

The processing of GPR data, as previously mentioned, produced an output radargram corrected in terms of signal noises and spatial representation. This corrected radargram is shown in Fig. 9 where the horizontal x-axis represents the progressive number of acquired traces (from acquisition nr. 0 to nr. 951) and the vertical y-axis represents the altitude in meters. Here, the vertical red line indicates the crossing with section A–A' of Fig. 6 (in correspondence of trace nr. 739) used for the slope stability analysis.

The processed radargram shows two main materials with evident differences. The upper one is characterised by a chaotic distribution with lack of internal stratification, and it has been interpreted as the debris deposit. This internal texture is consistent with the characteristics observed during field survey and described in the geological-structural map (Fig. 2). The lower material shows a relative homogeneity without stratification and has been interpreted as the micaschists bedrock. In addition, between the two materials there is evidence of a gradual transition that can be connected to the superficial alteration of the bedrock. Thus, the interface was considered within the gradual transition between the two materials at a depth of about 16 meters from the surface. This value was then used in the settings for the slope stability analysis in relation to the debris deposit thickness. However, it can be noted that the depth of the contact surface between the debris deposit and the bedrock is not constant along the acquisitions; somewhere, the depth increases probably due to the presence of impluvium orthogonally oriented in respect to the river creek filled by the debris.

The limit of the GPR acquisition with the selected settings was identified at a depth of about 22 meters from the surface (Fig. 9).

The strong and deep signal received at the beginning of the acquisition path, between trace n. 0 and n. 25, in Fig. 9, should not be considered because
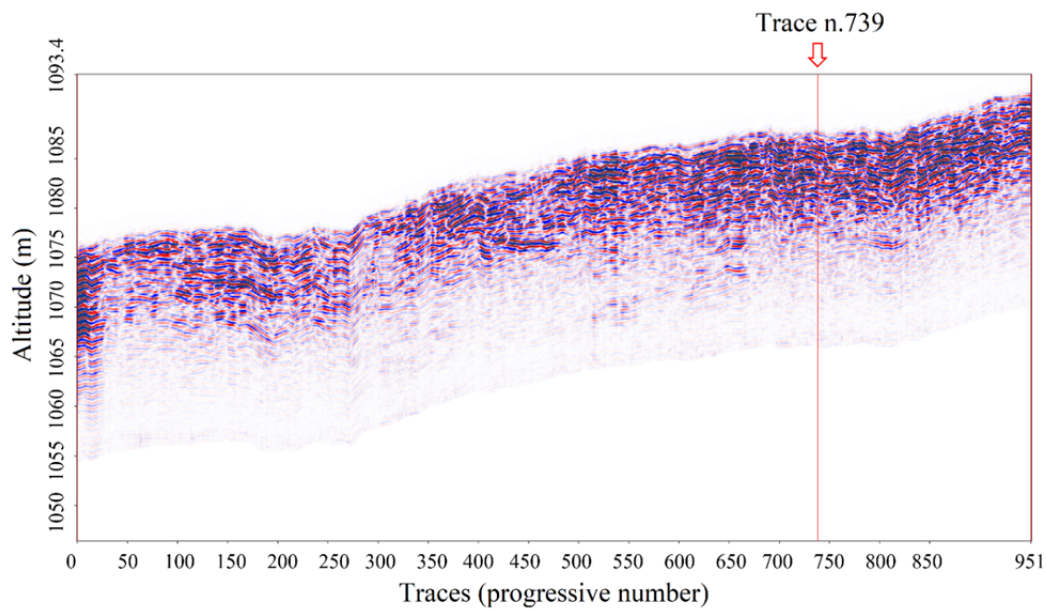
Fig. 9 GPR detection profile along the UAV path. The red line indicates the acquisition n. 739, in correspondence to the A–A' cross-section of Fig. 6.

it is caused only by the initial radar emitted energy. Therefore, this phenomenon hides the real bedrock depth in that area.

4.3 Scree slope stability analysis

The calculation of FoS for the slope modelled along the A–A' cross-section of Fig. 6 was carried out considering different scenarios: natural static condition, static condition with the presence of a snow cover (maximum load of 4.01 kN/m²), dynamic condition under seismic action, and, finally, dynamic condition considering both snow cover and seismic action. Fig. 10 shows the FoS as computed along the simplified slope under different conditions.

In the "Interpret" program of Slide2© the most probable failure surface from the simulations can be identified thanks to a coloured representation of results. The clusters of points above the slope in Fig. 10C and 10D represent the centres of rotation used for moment equilibrium calculations giving FoS values < 1.

The specific FoS values obtained for the different simulated scenarios are summed up in Table 3.

The results summed up in Table 3 show two different outputs: static conditions, both with and without snow cover, have FoS values lightly greater than 1 indicating the equilibrium of the slope; dynamic conditions (i.e., under seismic action and seismic action with snow cover) have FoS values lightly below the stability limit value of 1. Therefore, it

Table 3 FoS values resulting from the slope stability analysis in Slide2© (bold numbers indicate FoS values lower than 1)

Scenario	FoS
Natural static condition	1.033
Static condition and snow cover	1.040
Dynamic condition under seismic action	**0.938**
Dynamic condition under seismic action and snow cover	**0.953**

could be stated that reaching critical conditions (i.e., FoS value < 1) happens only when the dynamic seismic input is applied to the slope model.

5 Discussions

The study area described in the present work, located in a severe alpine environment, is characterised by steep slopes with the presence of rock boulders making the traditional geological survey difficult and dangerous to be conducted. These conditions led to the application of a coupled configuration of UAV-mounted GPR that, in parallel with the topographic and photogrammetric surveys, and the availability of geological maps and information, allowed the identification of the interface between the debris deposit and the bedrock and to assess the scree slope stability.

As far as processing of GPR data is concerned, the results were considered satisfactory since, among other things, it permitted to filter out, from the data
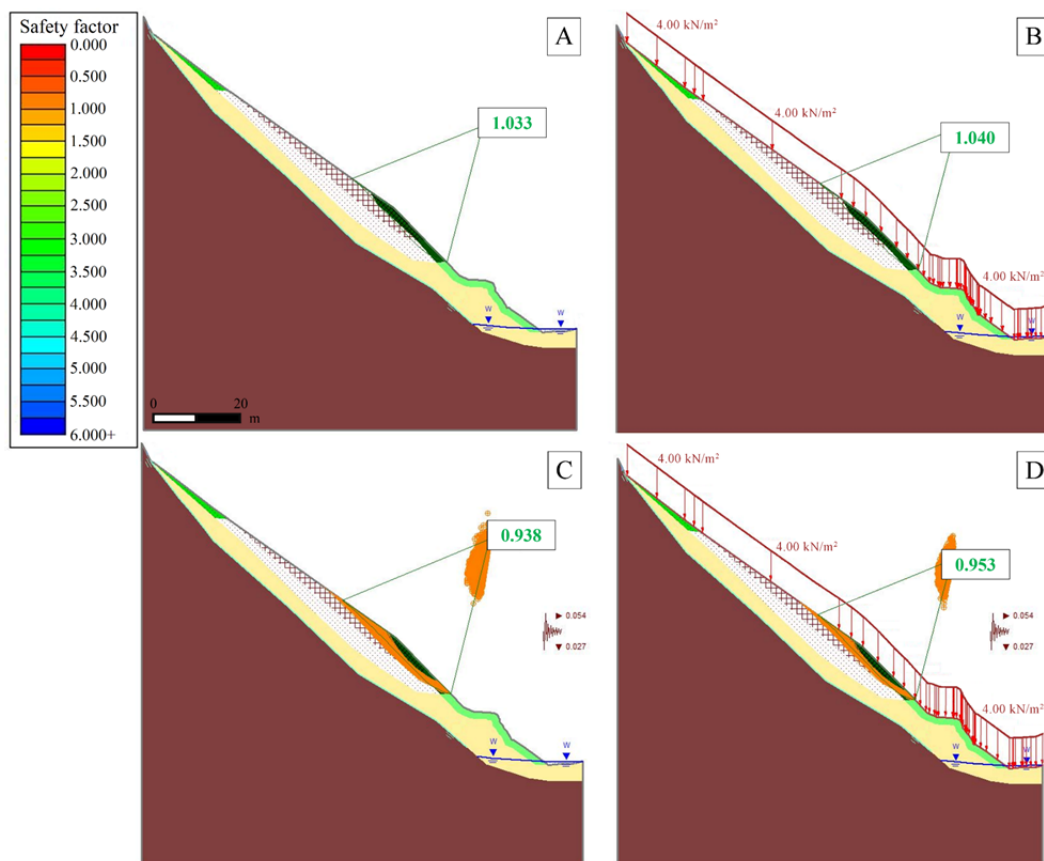
Fig. 10 Results of the slope stability analysis in natural static conditions (A), in static conditions with the presence of a snow cover (B), in dynamic conditions under seismic action (C), in dynamic conditions – under seismic action – and with the presence of the snow cover (D).

signal component, frequencies outside the bandwidth of the GPR system, hence enhancing the signal-to-noise ratio. Specifically, according to Pipan et al. (2020) background removal was used to take out the direct signal coming from the transmitter antenna as well as to reduce the magnitude of ringing and horizontal banding artifacts throughout the whole signal. The Ormsby bandpass filter allowed to suppress low-frequency interference and the signal's high-frequency components from the trace spectrum. The filtering was chosen to highlight those frequencies within the instrument's bandwidth where most of the energy is located, removing the influence of high and low-frequency noise. As part of the data processing procedure, the gain adjustment resulted extremely useful in compensating the signal exponential attenuation with depth, due to absorption, spherical divergence, and scattering phenomena. It allowed to equalize the amplitude of the electromagnetic waves which typically decreases with depth faster than seismic waves (Bianchini Ciampoli et al. 2019). The topographic correction was

applied to pass from a false flat cross-section to a corrected radargram with a realistic interface reflection depth. The definition of the interface between materials (i.e., upper debris deposit versus lower micaschists bedrock) resulted optimal and was defined at about 16 meters in correspondence of the intersection between the slope model section A-A' and the GPR acquisition path (Fig. 6). The interface depths in other points along the slope model, were determined by the interpretation of the geological-structural maps (Camanni 2010; Comunità Montana del Pinerolese 2015).

The data from the GPR, together with ones from the topographic and photogrammetric surveys, allowed us to create a slope model used to assess its stability in different natural conditions. The model creation included the presence of vegetation roots and their contribution in the total cohesion value. This choice was due to the fact that the slope is characterised not only by a coarse deposit made of block debris, but in some areas, it has a varied vegetation (trees, low bushes and grass) that increases

the material cohesion. Hence, the model was divided into zones in order to consider the granulometric and lithological characteristics and the presence of different vegetation types.

From the stability analysis it was possible to observe how the slope is in equilibrium in static conditions, even in presence of snow coverage which additional load favours the material compaction along the slope and could increase stability. In fact, compaction enhances the cohesion between material particles, making it more resistant to displacement and sliding. This could help to reduce the risk of collapses or landslides along the slope. Meanwhile, dynamic conditions (such as the occurrence of an earthquake), imply a reduction of the FoS values leading to slope instability. Thus, the actual slope conditions are at the limit of equilibrium: a disturbance of the static conditions (of any nature) could quickly cause a loss of balance with a possible consequent slope failure and creek blockage.

In light of the obtained results, some improvements to the present analysis that could be implemented in the near future can be highlighted. For example, it must be remembered that the presented slope model is based on a single radargram, and the stability analysis is conducted along one single cross-section. Hence, from the 2D numerical simulation it is possible to obtain the FoS and the potential failure surface only for that particular cross-section and, consequently, it may be too conservative. Therefore, to improve the completeness of the stability study and in relation to the already available data (ex., three-dimensional model of the slope and additional radargrams), a 3D stability analysis could be performed.

Despite the promising results of the coupled asset of a GPR mounted on drone, it should be addressed that this technique suffers from some constraints, such as the need of a reduced height between the coupled asset and the ground (Booth and Koylass 2022). Indeed, the energy transmitted by the GPR could be affected by a loss of reflectivity due to the impedance mismatch between air and ground (Garcia-Fernandez et al 2020; Francke and Dobrovolskiy 2021; Li et al. 2023), and by signal interferences at the interface and within the subsurface (Diamanti and Annan 2017; Edemsky et al. 2021).

In addition, when the drone is set to fly at higher elevation from the ground, the swath width increases with an upward rising reflection of electromagnetic waves. These could have angles of reflection away from the GPR receiver leading to an expanding dispersion of returning signals (Francke 2022). Also, the lateral spatial resolution can degrade with the increasing height due to the waves spreading through the air (Diamanti and Annan 2017; Garcia-Fernandez et al 2020). The latter is also considered the cause for the decreasing propagation through the ground when the wave is not normally penetrating the ground surface (Lau et al. 1992). Several studies recommended a height between 0.50 and 1.5 times the dominant wavelength of the radar wavelet (Diamanti and Annan 2017; Garcia-Fernandez et al 2018b; Šipoš and Gleich 2020; Garcia-Fernandez et al 2020).

Considering the CF of the used antenna (i.e., 124 MHz), which corresponds to a dominant wavelength of 2.4 m, and the above-mentioned working limitations, in this paper, it was decided to adopt an average drone fly height of 0.50 meters.

Another downside, which was experienced during the presented survey, is related to the difficulty of conducting the drone at an extremely low elevation from the surface and in steep areas characterized by the presence of diverse vegetation (scattered trees and low bushes) and rock boulders of diverse sizes. These conditions can be problematic and dangerous, both for the drone itself and for the operator, because the drone could be out of the direct operator's sight due to the presence of an obstacle in-between. In the present study case, it was preferred to conduct the drone manually, and not with the autonomous mission flight, in order to have full control along the chosen fly path and to avoid possible dangerous situations.

Other authors, in different areas characterized by similar inaccessibility and dangerous conditions for operators, report on the use of this survey method in different applications (McCallum and Fairweather 2013; Tan et al. 2017; Briggs et al. 2018; Eckerstorfer et al. 2018; Garcia-Fernandez et al. 2018a; Garcia-Fernandez et al. 2019a; Garcia-Fernandez et al. 2019b; Šipoš and Gleich 2020; Jensen et al. 2020; Garcia-Fernandez et al. 2022). A similar configuration is also proved to be useful when site access is forbidden, or the surface conditions must be preserved as, for example, agricultural or archaeological areas (Yarleque et al. 2017; Hou et al. 2021; Colica et al. 2022).

6　Conclusions

The development of sensors and remote detection techniques that can be mounted on vehicles has had a rapid evolution in the last decade. The newest methodologies can benefit from high-performance instrumentations, tools, hardware, and software. In addition, the possibility of integrating devices, such as thermal cameras, multispectral cameras, hyperspectral scanners, and laser scanners, with UAVs has been widening the application range for these technologies. While the geological application of ground-based GPR has been mainly focused on the definition of bedrock depth, underground setting and on the identification of fractures, buried structures, and ground water level, the use of a UAV-mounted GPR can open to novel frontiers even in inaccessible areas.

The present case study, for instance, refers to a scree slope whose access was restricted for security reasons. A methodological approach for detrital slope stability analysis is hereby presented by exploiting the advantages of an innovative GPR-drone technology and with the support of the photogrammetric technique. Indeed, while the latter allowed to produce the 3D point cloud, DDTM and orthophotos of the slopes, the GPR-drone integrated system permitted to define the interface between bedrock and the detrital deposit. These coupled methodologies were used to analyse slope stability efficiently and the results can be used to assess the site safety.

A potential future application of this technique could be related to slope stability 3D modelling after the execution of UAV-GPR flights according to a grid pattern instead of lines. This working schedule could allow to investigate the depth of the bedrock under a detrital deposit in 3D and to build a model for assessing the stability of slopes not only along cross-sections but at the entire study area scale.

Moreover, a periodical monitoring of the scree slope could be implemented in such a way as to assess its stability through time: the slope can modify its shape and characteristics under weather conditions (ex., extreme rainfalls, snow cover, ice), human activities, and seismic action.

In addition, we are currently working on the improvement of radargram processing for automatic detection of discontinuities from GPR traces. Thereby, it will be possible to further benefit from advantages related to the application of the drone-

GPR method, particularly at sites where local geological information on stratigraphy or geophysical surveys are missing.

Next foreseen applications will involve the investigation of bedrock surface in different environments such as dump deposits of open pit mines and quarries, natural slopes covered by soils, and artificial slopes in drained dam reservoirs. This will provide a frame of reference for the same GPR-drone integrated technique, combined with topographic and photogrammetric surveys, for different geometrical and geological conditions, leading to a multi-techniques approach useful to verify natural and anthropic slope stability.

Undertaking GPR-UAV surveys in complex geographic conditions represents a big challenge for scientists and professionals in their efforts to deal with complex topographic environments. Thus, this work shows the advantages of using a powerful instrument like that of the drone, which can fly either manually or autonomously, whilst assuring precise results and safe conditions during fieldwork operations.

Author Contributions

R.S. is the Unit Project Coordinator for the University of Siena; C.V. and A.R. conducted topographic surveys through GNSS and TS, and the UAV-GPR survey. R.S., D.S., C.V., and A.R. conducted the processing of topographic and photogrammetric data. L.B., V.D.L., A.E., and C.V., processed the radar

data. R.S., L.B., V.D.L., A.E., and C.Z., analysed the scree slope stability. All the authors contributed to the text writing. All authors have read and agreed to the published version of the manuscript.

Ethics Declaration

Conflict of Interest: The authors declare no conflict of interest.

Open Access

References

Abudeif AM, Abdel al GZ, Masoud MM, et al. (2022) A Geoarchaeological investigation of Abydos area using land magnetic and GPR techniques, El-Balyana, Sohag, Egypt. Appl Sci 12 (19): 9640.
https://doi.org/10.3390/app12199640

Al-Ruzouq R, Abu Dabous S, Abueladas A, et al. (2022) Integrated archaeological modeling based on geomatics techniques and Ground-Penetrating Radar. Remote Sens 14 (7): 1622. https://doi.org/10.3390/rs14071622

Azahar MA, Rusli QN, Salleh MA, et al. (2018) The use of non-invasive geophysical techniques in detecting of boulder and bedrock at Pulau Pangkor, Perak, Malaysia. Electron. J Geotech Eng 23.

Bandini F, Kooij L, Karl Mortensen B, et al. (2022) Mapping inland water bathymetry with Ground Penetrating Radar (GPR) on board Unmanned Aerial Systems (UASs). J Hydrol 616: 128789. https://doi.org/10.1016/j.jhydrol.2022.128789

Bayisa R, Kumar RT, Seifu K (2015) Quarry site selection and geotechnical characterization of ballast aggregate for Ambo-Ijaji railway project in Central Ethiopia: An integrated GIS and geotechnical approach. In: Lollino G et al. (eds.), Engineering Geology for Society and Territory. Springer International Publishing Volume 6. Cham, Germany. pp 329-335. https://doi.org/10.1007/978-3-319-09060-3_56

Bertea A (1989) Geologia e struttura del giacimento di talco Fontane (Val Germanasca - Alpi Cozie). Tesi di Laurea in Scienze Geologiche, Università di Torino, Dipartimento di Scienze della Terra; Torino. (In Italian).

Bianchini Ciampoli L, Tosti F, Economou N, et al. (2019) Signal processing of GPR Data for road surveys. Geosciences 9(2): 96. https://doi.org/10.3390/geosciences9020096

Bishop AW (1955) The use of the slip circle in the stability analysis of slopes. Géotechnique 5(1): 7-17.
https://doi.org/10.1680/geot.1955.5.1.7

Booth AD, Koylass TM (2022) Drone-mounted Ground-Penetrating Radar surveying: flight-height considerations for diffraction-based velocity analysis. Geophysics 87 (4): 69-79.
https://doi.org/10.1190/geo2021-0602.1

Briggs R, Thibault C, Mingo L (2018) Usage of unmanned aerial vehicles for iceberg surveying and monitoring - Preliminary results. In: OTC Arctic Technology Conference. OnePetro.
https://doi.org/10.4043/29132-ms

Buchanan P, Savigny KW (1990) Factors controlling debris avalanche initiation. Can Geotech J 27: 659-675.
https://doi.org/10.1139/t90-079

Cadoppi P, Camanni G, Balestro G (2016) Geology of the fontane talc mineralization (Germanasca Valley, Italian Western Alps). J Maps 12 (5): 1170-1177.
https://doi.org/10.1080/17445647.2016.1142480

Camanni G (2010) Geological-Structural Analysis and 3D modelling of the fontane talc mineralization Germanasca Valley, Inner Cottian Alps. Tesi di Laurea Magistrale in Scienze Geologiche, Università di Torino, Facoltà di Scienze Naturali, Fisiche e Matematiche, Torino. (In Italian).

Chok YH, Jaksa MB, Kaggwa WS, et al. (2015) Assessing the influence of root reinforcement on slope stability by finite elements. Int J Geo-Eng 6(1).
https://doi.org/10.1186/s40703-015-0012-5

Colica E, D'Amico S, Luciano G, et al. (2022) Integrated geophysical and geomatics study at Xrobb L-Ghagin archaeological site: preliminary results. J Phys Conf Ser 2204 (1): 012088.
https://doi.org/10.1088/1742-6596/2204/1/012088

Comunità Montana del Pinerolese (2015) Piano regolatore generale intercomunale - carta dei caratteri litotecnici e idrogeologici. 81. (In Italian).

Coppin N J, Richards IG (2007) Use of vegetation in civil engineering. Ciria: Editora. London.

Coulomb, CA (1973) Essai sur une application des règles des maximis et minimis a quelquels problèmes de statique, relatifs a la architecture. Mem Acad R Div Sav 7L. pp 343-387. (In French).

D.G.R. n. 6-887 UPCM 3519/2006 of 30 December 2019. Presa d'atto e approvazione dell'aggiornamento della classificazione sismica del territorio della regione Piemonte, di cui alla D.G.R. del 21 maggio 2014 n. 65-7656". Available online:
https://www.geologipiemonte.it/comunicazioni/regione-piemonte/articolo/d-g-r-n-6-887-del-30-12-2019 (Accessed

on 9 October 2023). (In Italian).

Diallo MC, Cheng LZ, Rosa E, et al. (2019) Integrated GPR and ERT data interpretation for bedrock identification at Cléricy, Québec, Canada. Eng Geol 248: 230-241. https://doi.org/10.1016/j.enggeo.2018.09.011

Diamanti N, Annan AP (2017) Air-launched and ground-coupled GPR data. 11th European conference on antennas and propagation (EUCAP) 2017. https://doi.org/10.23919/eucap.2017.7928409

Eckerstorfer M, Jenssen ROR, Kjellstrup A, et al. (2018) UAV-borne UWB radar for snowpack surveys. Project report, Northern Research Institute (NORUT).

Edemsky D, Popov A, Prokopovich I, et al. (2021) Airborne Ground Penetrating Radar, field test. Remote Sens 13(4): 667. https://doi.org/10.3390/rs13040667

Elkarmoty M, Tinti F, Kasmaeeyazdi S, et al. (2018) Implementation of a fracture modeling strategy based on georadar survey in a large area of limestone quarry bench. Geosciences 8 : 481. https://doi.org/10.3390/geosciences8120481

Emilsson J, Friborg J, Gustafsson J, et al. (2022) On the development and application of airborne GPR solutions. First break 40(8): 47-54. https://doi.org/10.3997/1365-2397.fb2022065

Essam D, Ahmed M, Abouelmagd A, et al. (2020) Monitoring temporal variations in groundwater levels in urban areas using ground penetrating radar. Sci Total Environ 703: 134986. https://doi.org/10.1016/j.scitotenv.2019.134986

Feiger N, Huss M, Leinss S, et al. (2018) The bedrock topography of gries and findelengletscher. Geogr Hel 73(1):1-9. https://doi.org/10.5194/gh-73-1-2018

Francke J (2022) Advancements in Ground Penetrating Radar technology for mineral exploration. In: GeoConvention, Calgary. Canada. 20-22 June 2022.

Francke J, Dobrovolskiy A (2021) Challenges and opportunities with drone-mounted GPR. In: First international Meeting for Applied Geoscience & Energy Expanded Abstracts. https://doi.org/10.1190/segam2021-3582927.1

Fuente JV, Diego R, Fabregad R (2021) Ground Penetrating Radar survey for the location and assessment of the hydrocarbon plumes at gas station installations. J Geosci and Environ Prot 09(12): 57-71. https://doi.org/10.4236/gep.2021.912004

Garcia-Fernandez M, Alvarez Lopez Y, De Mitri A (2020) Portable and easily-deployable air-launched GPR scanner. Remote Sens 12 (11): 1833. https://doi.org/10.3390/rs12111833

Garcia-Fernandez M, Alvarez-Lopez Y, Heras FL, et al. (2018a) GPR system onboard a UAV for non-invasive detection of buried objects. In: IEEE International symposium on antennas and propagation & USNC/URSI National Radio Science Meeting. https://doi.org/10.1109/apusncursinrsm.2018.8608907

Garcia-Fernandez M, Alvarez-Lopez Y, Las Heras F (2019a) Autonomous airborne 3D SAR imaging system for subsurface sensing: UWB-GPR on board a UAV for landmine and IED detection. Remote Sens 11: 2357. https://doi.org/10.3390/rs11202357

Garcia-Fernandez M, Alvarez-Narciandi G, Alvarez-Lopez Y, et al. (2022) Validation of a UAV-Mounted GPR system for landmine and IED detection under operational conditions. In: Chemical, Biological, Radiological, Nuclear, and Explosives (CBRNE) Sensing XXIII. https://doi.org/10.1117/12.2622925

Garcia-Fernandez M, Lopez YA, Arboleya AA (2018b) Synthetic Aperture Radar imaging system for landmine detection using a Ground Penetrating Radar on board a Unmanned Aerial Vehicle. IEEE Access 6: 45100-45112. https://doi.org/10.1109/ACCESS.2018.2863572

Garcia-Fernandez M, Morgenthaler A, Alvarez-Lopez Y, et al. (2019b) Bistatic landmine and IED detection combining vehicle and drone mounted GPR sensors. Remote Sens 11: 2299. https://doi.org/10.3390/rs11192299

GeoStru (2022). Free online Application. http://geoapp.eu/parametrisismici2018/ (Accessed on 9 October 2023).

Gomes K, Oliva P, Rocha H, et al. (2022) Evaluation of the contamination of the subsurface and groundwater by monoaromatic hydrocarbons in an Eastern amazonian town in Northern Brazil. Environ Earth Sci, Preprint version. https://doi.org/10.21203/rs.3.rs-1559646/v1

GPL Software (2022). CloudCompare, Version 2.9.1 2022. http://www.cloudcompare.org/ (Accessed on 9 October 2023).

Grandjean G, Gourry JC (1996) GPR data processing for 3D fracture mapping in a marble quarry (Thassos, Greece). J Appl Geophys 36: 19-30. https://doi.org/10.1016/S0926-9851(96)00029-8

Gray DH, Leiser AT (1982) Biotechnical slope protection and erosion control. Krieger Publishing Company.

Guireli Netto L, Barbosa AM, Galli VL, et al. (2020) Application of invasive and non-invasive methods of geo-environmental investigation for determination of the contamination behavior by organic compounds. J Appl Geophys 178: 104049. https://doi.org/10.1016/j.jappgeo.2020.104049

Guo J, Li L, Liu J, et al. (2022) Ground-Penetrating Radar survey of subsurface features at the margin of ice sheet, East Antarctica. J Appl Geophys 206: 104816. https://doi.org/10.1016/j.jappgeo.2022.104816

Hall N, Fischer A, Uchytil G, et al. (2022) Holocaust archaeology: GPR subsurface imaging of the mila 18 memorial in Warsaw, Poland. In: 19th International Conference on Ground Penetrating Radar. https://doi.org/10.1190/gpr2022-055.1

Hou J, Yan Y, Cong P (2021) Application of technology of UAV-mounted Ground Penetrating Radar in the study of the thickness of soil plow layer. IOP Conf Ser: Earth Environ Sci 719(4): 042074. https://doi.org/10.1088/1755-1315/719/4/042074

Hussain Y, Uagoda R, Borges W, et al. (2020) The potential use of geophysical methods to identify cavities, sinkholes and pathways for water infiltration. Water 12(8): 2289. https://doi.org/10.3390/w12082289

Jenssen ROR, Eckerstorfer M, Jacobsen S (2020) Drone-Mounted ultrawideband radar for retrieval of snowpack properties. IEEE Trans Instrum Meas 69(1): 221-230. https://doi.org/10.1109/tim.2019.2893043

Jol HM (2009) Ground Penetrating Radar theory and applications, 1st ed. Elsevier Science. Burlington, Vermont, USA. p 544. https://doi.org/10.1016/B978-0-444-53348-7.X0001-4

Kulich J, Bleibinhaus F (2020) Fault detection with crosshole and reflection geo-radar for underground mine safety. Geosciences 10: 456. https://doi.org/10.3390/geosciences10110456

Lau C, Scullion T, Chan P (1992) Modeling of Ground-Penetrating Radar wave propagation in pavement systems. Transp Res Rec 1355: 99-107.

Li B, Yang H, Guo L, et al. (2023) A dual-band antireflection metasurface for air-ground impedance matching in Ground Penetrating Radar. Phys Scr 98(3): 035515. https://doi.org/10.1088/1402-4896/acbbb1

Liu J, Wang S, He Y, et al. (2020) Estimation of ice thickness and the features of subglacial media detected by Ground Penetrating Radar at the Baishui river glacier no. 1 in Mt. Yulong, China. Remote Sens 12(24): 4105. https://doi.org/10.3390/rs12244105

Ludeno G, Catapano I, Gennarelli G, et al. (2017) A micro-UAV-borne system for radar imaging: A feasibility study. In: 9th International workshop on advanced Ground Penetrating Radar (IWAGPR). https://doi.org/10.1109/iwagpr.2017.7996034

Maryadi M, Supriyanto, Champai FMS, et al. (2020) Analysis of groundwater contamination level in residential areas around

Cipayung landfill using Ground Penetrating Radar. IOP Conf Ser: Mater Sci Eng 874(1): 012013. https://doi.org/10.1088/1757-899x/874/1/012013

McCallum AB, Fairweather H (2013) UAV-mounted GPR for remote area radioglaciology. In: International symposium on radioglaciology, Lawrence, United States, 09-13 September 2013.

Miccinesi L, Beni A, Pieraccini M (2022) UAS-borne radar for remote sensing: a review. Electronics 11(20): 3324. https://doi.org/10.3390/electronics11203324

Nath RR, Kumar G, Sharma ML, et al. (2018) Estimation of bedrock depth for a part of Garhwal Himalayas using two different Geophysical Techniques. Geosci Lett 5(1). https://doi.org/10.1186/s40562-018-0108-9

Novo A, Sala R, Kauffman M, et al. (2021) High-resolution GPR investigation over a Roman mosaic in Empuries, Spain. In: 11th International Workshop on Advanced Ground Penetrating Radar (IWAGPR). https://doi.org/10.1109/iwagpr50767.2021.9843149

Onyebueke E, Manzi M, Gomo S, et al. (2022) Boulder delineation using integrated GPR and electrical resistivity method at Tharisa platinum mine, Rustenburg, South Africa. In: NSG2022 4th Conference on Geophysics for Mineral Exploration and Mining. https://doi.org/10.3997/2214-4609.202220181

Peterson CD, Doliber SR (2019) Groundwater Surface (GWS) mapping by Ground Penetrating Radar (GPR) for use in protecting freshwater habitats, water quality, and active dune landscapes, in the Florence coastal dune sheet, Oregon, USA. J Geogr Geol 11(1): 13. https://doi.org/10.5539/jgg.v11n1p13

Pipan M, Baradello L, Forte E, et al. (2020) GPR study of bedding planes, fractures, and cavities in limestone. In: Noon DA, Stickley GF, Longstaff D (eds.), Eighth international conference on Ground Penetrating Radar, Gold Coast, Australia, 23-26 May. pp 682-687. Available online: https://www.spiedigitallibrary.org/conference-proceedings-of-spie/4084/0000/GPR-study-of-bedding-planes-fractures-and-cavities-in-limestone/10.1117/12.383499.short?SSO=1 (Accessed on 9 October 2023).

Prager S, Sexstone G, McGrath D (2022) Snow depth retrieval with an autonomous UAV-mounted software-defined radar. IEEE Trans Geosci Remote Sens 60: 1-16. https://doi.org/10.1109/tgrs.2021.3117509

Qin T, Zhao Y, Lin G, et al. (2018) Underwater archaeological investigation using Ground Penetrating Radar: a case analysis of Shanglinhu Yue Kiln Sites (China). J Appl Geophy 154: 11-19. https://doi.org/10.1016/j.jappgeo.2018.04.018

Radar Systems Inc. (2021) Prism2, Version 2.70.04. Darzauglu str. 1-105, Riga, Latvia. https://www.radsys.lv/en/index/ (Accessed on 9 October 2023).

RocScience Inc. (2022) Slide2, 2D Geotechnical Finite Element Analysis, Version 11.015. Toronto, ON, Canada, 2021. https://www.rocscience.com/ (Accessed on 9 October 2023).

Sarkar S, Roy A K, Raha P (2016) Deterministic approach for susceptibility assessment of shallow debris slide in the Darjeeling Himalayas, India. Catena 142: 36-46. https://doi.org/10.1016/j.catena.2016.02.009

Saponaro A, Dipierro G, Cannella E, et al. (2021) A UAV-GPR fusion approach for the characterization of a quarry excavation area in Falconara Albanese, Southern Italy. Drones 5: 40. https://doi.org/10.3390/drones5020040

Shukla S B, Chowksey VM, Prizomwala SP, et al. (2013) Internal sedimentary architecture and coastal dynamics as revealed by Ground Penetrating Radar, Kachchh Coast, Western India. Acta Geophys 61 (5): 1196-1210.

https://doi.org/10.2478/s11600-013-0102-8

Šipoš D, Gleich D (2020) A lightweight and low-power UAV-borne Ground Penetrating Radar design for landmine detection. Sensors 20(8): 2234. https://doi.org/10.3390/s20082234

Sonkamble S, Chandra S (2021) GPR for earth and environmental applications: case studies from India. J Appl Geophys 193: 104422. https://doi.org/10.1016/j.jappgeo.2021.104422

Tan A, Eccleston K, Platt I, et al. (2017) The design of a UAV mounted snow depth radar: results of measurements on Antarctic Sea Ice. In: IEEE Conference on Antenna Measurements & Applications (CAMA). https://doi.org/10.1109/cama.2017.8273437

Technical Standards for Construction (NTC 2018) approved by Ministerial Decree of 17/01/2018. (In Italian) https://www.gazzettaufficiale.it/eli/gu/2018/02/20/42/so/8/sg/pdf (Accessed on 9 October 2023).

Tomecka-Suchoń S, Gołębiowski T, Dec J, et al. (2019) Application of GPR and seismic methods for non-invasive examination of glacial and postglacial sediments in the Psia Trawka Glade: The Tatra Mts, Poland. Acta Geophys 67(6): 1777-1789. https://doi.org/10.1007/s11600-019-00334-x

Vanneschi C, Rindinella A, Salvini R (2022) Hazard assessment of rocky slopes: an integrated photogrammetry-GIS approach including fracture density and probability of failure data. Remote Sens 14: 1438. https://doi.org/10.3390/rs14061438

Vergnano A, Franco D, Godio A (2022) Drone-borne Ground-Penetrating Radar for snow cover mapping. Remote Sens 14(7): 1763. https://doi.org/10.3390/rs14071763

Wang S, Tan H (2018) Numerical simulation of groundwater pollution model by GPR. In: AGU fall meeting, NASA ADS 2018, NS31C0764. Available online: https://ui.adsabs.harvard.edu/abs/2018AGUFMNS31C0764W (Accessed on 9 October 2023).

Wu K, Rodriguez GA, Zajc M, et al. (2019) A new drone-borne GPR for soil moisture mapping. Remote Sens Environ 235(9). https://doi.org/10.1016/j.rse.2019.111456

Yarleque MA, Alvarez S, Martinez HJ (2017) FMCW GPR Radar Mounted in a mini-UAV for archaeological applications: first analytical and measurement results. In: International Conference on Electromagnetics in Advanced Applications (ICEAA). https://doi.org/10.1109/iceaa.2017.8065606

Yu H, Kim B, Song SY, et al. (2021) Geophysical surveys in a LNAPL contaminated site in South Korea and integrated interpretation with borehole data. NASA ADS, NS15B0377. Available online: https://ui.adsabs.harvard.edu/abs/2021AGUFMNS15B0377Y (Acessed on 9 October 2023).

Zajc M, Urbanc J (2019) Using GPR on a problematic agricultural field for groundwater protection in a karst environment. In: 10th International Workshop on Advanced Ground Penetrating Radar. https://doi.org/10.3997/2214-4609.201902563

Zanzi L, Hojat A, Ranjbar H, et al. (2019) GPR measurements to detect major discontinuities at Cheshmeh-Shirdoosh limestone quarry, Iran. Bull Eng Geol Environ 78: 743-752. https://doi.org/10.1007/s10064-017-1153-x

Zhang D, Zhong R, Li JC (2014) Topographic correction of GPR profiles based on laser data. IOP Conf Ser: Earth Environ Sci 17: 012251. https://doi.org/10.1088/1755-1315/17/1/012251

Zhao Y, Ling C, Zhang K, et al. (2022) Detection of hidden mining-induced ground fissures via Unmanned Aerial Vehicle infrared system and Ground-Penetrating Radar. Int J Rock Mech Min Sci 160: 105254. https://doi.org/10.1016/j.ijrmms.2022.105254